Quantum Chemical Investigation of Low-Temperature Intramolecular Hydrogen Transfer Reactions of Hydrocarbons

Jim Pfaendtner, Xinrui Yu, and Linda J. Broadbelt*

Department of Chemical and Biological Engineering, Northwestern University, Evanston, Illinois 60208-3120

Received: March 16, 2006; In Final Form: July 26, 2006

The B3LYP functional was evaluated as a method to calculate reaction barriers and structure−reactivity relationships for intramolecular hydrogen transfer reactions involving peroxy radicals. Nine different basis sets as well as five other MO/DFT and hybrid methods were used in comparing three reactions to available experimental data. It was shown that B3LYP/6-311+G(d,p) offers a good compromise between speed and accuracy for studies in which thermodynamic and kinetic data of many reactions are required. Sixteen reactions were studied to develop structure−reactivity relationships to correlate the activation energy with the heat of reaction. As long as no structural heterogeneities were present in the transition state ring, a simple Evans−Polanyí relationship was shown to capture the activation energy as a function of heat of reaction for reactions in the 1,5-hydrogen shift family. For peroxy radicals undergoing self-abstraction of a hydrogen atom in the 1,5-position, the activation energy was calculated as E_a (kcal mol^{-1}) = 6.3 + ΔH_{rxn} (kcal mol^{-1}). For reactions with a carbonyl group embedded in the ring of the transition state, the activation energy of peroxy radicals undergoing self-abstraction was correlated as E_a (kcal mol^{-1}) = 18.1 + 0.74*ΔH_{rxn} (kcal mol^{-1}). The impact of the size of the transition state ring on the activation energy and pre-exponential factor was also probed, and it was shown that these effects can be described using simple nonlinear and linear fits, respectively.

1. Introduction

The low-temperature oxidation of hydrocarbons is of interest to researchers in a number of different fields. Examples include the oxidative degradation of lubricating oils[1,2] and combustion of fuels in novel engines.[3] Despite decades of detailed experimental and theoretical investigations, a number of fundamental questions remain unanswered about elementary step reaction networks that can describe the low-temperature condensed-phase oxidation of large hydrocarbons. One main obstacle in answering these questions is the accurate resolution of the kinetic parameters of the important elementary reactions.

The fundamental reaction pathways in condensed-phase oxidation are basically well established and have been reviewed extensively including recent comprehensive reviews by Emanuel and Gál[4] and Denisov and Denisova.[5] However, successful generation of a large-scale complex reaction network requires kinetic data for hundreds or thousands of reactions, and in the case of condensed-phase oxidation, published data can be contradictory or lacking altogether. Therefore, the use of kinetic correlations, or structure−reactivity relationships, has become widespread in the modeling community as a means of estimating rate coefficients of reactions in large-scale mechanisms. In the case of bimolecular atom-transfer reactions, the Blowers−Masel correlation has been shown to be particularly effective in estimating the activation energy.[6] The Blowers−Masel correlation is an improvement upon the classic Evans−Polanyí correlation,[7] which has been shown to work well for a number of different elementary reaction types in free radical chemistry.[8−10]

One reaction class that is of particular interest in the early phase of oxidation is intramolecular hydrogen transfer.[11] These reactions are driven by the growth of peroxy radicals ($RO_2^{\bullet}$), which are formed from the very fast addition of molecular oxygen to primary radical species. Subsequent isomerization of $RO_2^{\bullet}$ species leads to hydroperoxyalkyl radicals ($^{\bullet}$QOOH) that are able to directly yield molecular products or introduce bifunctional moieties along the hydrocarbon backbone. Wijaya et al.[3] have recently performed a thorough investigation of the fate of $^{\bullet}$QOOH in the low-temperature regime. Herein we investigate the isomerization reactions that lead to the formation of $^{\bullet}$QOOH.

Intramolecular hydrogen transfer reactions of $RO_2^{\bullet}$ species are difficult to study experimentally, and kinetic parameters must often be inferred from data rather than directly measured. Denisova and Denisov[12] tabulated a number of the experimentally available rate constants for unimolecular hydrogen shifts of peroxy radicals. In their review of condensed-phase oxidation, Mill and Hendry[13] give accepted experimental values for the pre-exponential factor of intramolecular abstraction by peroxy radicals of log *A* (1/s) equal to 12.5, 11.5, and 11.0 for ring sizes (transition state) of 5, 6, and 7, respectively. Van Sickle and co-workers studied the 1,5-hydrogen shift (six-membered ring formed) of 2-peroxy pentane.[14] They reported a unimolecular rate constant of 0.87 s^{-1} at 373 K. The 1,5-hydrogen shift of 2-peroxy-2,4-dimethylpentane was reported by Mill and Montorsi[15] to have a rate constant of 18 s^{-1} at 373 K. Mill and Hendry[13] derived a rate constant of 8 s^{-1} at 373 K from the data of Rust[16] for the 1,6-hydrogen shift of 2-peroxy-2,5-dimethylhexane. Given the experimentally accepted rate constants and pre-exponential factors, it is possible to derive activation energies of 19.7, 17.5, and 17.2 kcal mol^{-1} for these three reactions, respectively.

There have been few attempts to theoretically characterize the intramolecular hydrogen shift reactions of peroxy radicals. Denisova and Denisov[12] estimated activation energies by

* Corresponding author phone: (847) 491-5351; Email: broadbelt@northwestern.edu.

10.1021/jp061649e CCC: $33.50
Published on Web 08/25/2006

applying an analogue of the Marcus equation. Their method requires a priori knowledge of both the dissociation energies as well as the frequencies of bonds being broken and formed in the reaction. To accurately apply this method to a wide range of systems, a rigorous quantum mechanical treatment would be necessary in order to obtain these unknown quantities. An alternative approach is to use transition state theory (TST) to obtain rate constants applicable in the condensed phase as well as in the high-pressure limit.

Quantum mechanical studies of this reaction class are limited to the works by Chan and co-workers[11] and Merle and co-workers.[17] Chan et al. studied the self-abstraction by peroxy radicals for a small series of aliphatic hydrocarbons using the BHandHLYP functional with a 6-311G(d,p) basis set. It was recently demonstrated[3] that BHandHLYP has the potential to be a predictive tool for studying kinetics of some peroxy radical reactions, but not without including corrections for internal rotation and errors associated with the peroxy ligand. Merle et al. studied the unimolecular isomerization of the *n*-propylperoxy radical using B3LYP/6-31+G(d,p) and CBS-QB3.

The purpose of the present work is to study the intramolecular hydrogen transfer of several peroxy radicals using quantum mechanical calculations. The effect of substituents and transition state (TS) ring size will be used to elucidate kinetic correlations suitable for calculating rate constants in the high-pressure limit. In the past several years, the B3LYP functional has been used extensively in similar kinetic studies. Balderas and co-workers have recently provided an extensive evaluation of many quantum mechanical methods for several addition reactions.[18] However, a broader consensus as to which basis set is appropriate for various systems is still lacking. To help guide selection of an appropriate method, we studied the three reactions for which experimental data is available as noted above using the B3LYP functional with seven different basis sets as well as BHandHLYP/6-311G(d,p), MP2/6-311+G(d,p), G3(MP2), G3//B3LYP, and CBS-QB3 methods. The BHandHLYP/6-311G(d,p) functional and basis set were selected for comparison with previously obtained results using this level of theory.[3,11] These reactions are pictured as reactions 1−3 in Figure 1. A larger set of reactions (reactions 4−11 in Figure 1) was studied at the B3LYP/6-311+G(d,p) level of theory to develop kinetic correlations for estimating rate constants or developing reaction mechanisms.

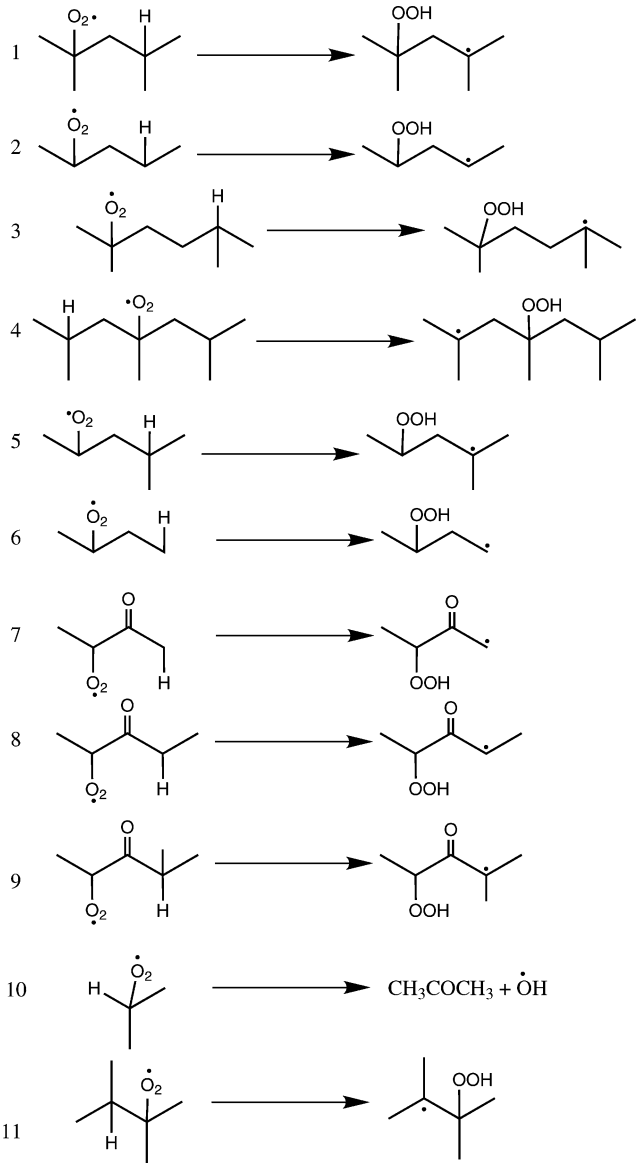

Figure 1. Intramolecular hydrogen abstraction reactions involving peroxy radicals studied using quantum chemistry. For brevity, each reaction is given a numerical identification.

2. Computational and Theoretical Details

All molecular orbital (MO) and density functional theory (DFT) calculations were completed using the Gaussian 03[19] software package. At each level of theory and basis set, the geometries of all reactants and products were optimized to minimum energy structures using the Berny algorithm.[20] Transition states were identified as first-order saddle points on the potential energy surface. After locating a TS of a particular ring size, other similar transition states were located efficiently and successfully using the quadratic synchronous transit (QST3)[21] method. All transition states were first validated by verification that only one large amplitude imaginary frequency was present in the proposed TS. The true reactant and product(s) corresponding to each TS were obtained by using intrinsic reaction coordinate following.[22]

Transition states were determined using a number of different MO and DFT prescriptions. In response to its immense popularity in the literature, we screened Becke's[23] three parameter hybrid functional, B3LYP, most extensively. Seven different basis sets were employed including Pople Gaussian-type basis sets as well correlation consistent basis sets of Dunning. Within the Pople formalism split-valence double and triple-ζ basis sets optionally including d, f, and p-type polarization functions on first or second row atoms as well as an optional single set of diffuse functions on first-row atoms were used. The different basis sets examined were: 6-31G(d), 6-31G(d,p), 6-311G(d,p), 6-311+G(d,p), 6-311+G(df), and 6-311+G(3df,-2p). For further comparison, restricted open-shell wave functions were used in two of the B3LYP cases; unless noted all calculations are done with unrestricted, open-shell wave functions. A single calculation using a correlation consistent basis set was carried out employing polarized valence triple-ζ functions augmented with diffuse functions (B3LYP/cc-pVTZ+d). Additionally, for comparison with results obtained previously,[3,11] the Becke[23] half and half functional, BHandHLYP, was used with a single basis set, 6-311G(d,p). Structures optimized using MP2/6-311+G(d,p) allowed further comparisons to be made. The results were additionally benchmarked using high-level extrapolation methods. Two composite methods that have been shown to provide accurate results in radical chemistry,[24] CBS-QB3[25] and G3//B3LYP,[26] were used. Calcula-

tions were also performed using G3(MP2)[27] in order to probe the effect of a high-level correction using MP2 optimized geometries. Accepted B3LYP scaling factors of 0.9806 for zero-point energies and 0.9614 for other calculations, e.g., partition functions, were used.[28] Scott and Radom optimized these scaling factors specifically for the 6-31G(d) basis set, but given the absence of scale factors for other basis sets, it has become commonplace to scale results using these values for B3LYP, regardless of the basis set.[17,29] Finally, solvation effects were studied using a polarizable continuum model (PCM).[30] The solvent cavity was established using radii obtained from the universal force field[31] with hydrogen atoms explicitly defined. Full geometry optimization and energy calculations were performed with *n*-heptane as the solvent using B3LYP/6-31G-(d).

Using the optimized geometry and frequencies obtained from a Hessian calculation, the total microcanonical partition function can be calculated for each molecule within the rigid-rotor harmonic oscillator (HO) assumption. The formulas for electronic, translational, rotational and vibrational partition functions are well established.[32] However, the HO approximation incorrectly treats low-frequency rotations as harmonic oscillators. If left uncorrected, this can induce substantial error in calculated kinetic and thermodynamic data. Internal rotations whose barrier to rotation is much less than kT are characterized as free rotors and corrected easily.[33] In the temperature range of interest to the current study (300−1000 K), the barrier to rotation for all dihedrals is on the order of kT, therefore requiring that internal rotations be treated as hindered rotors. Our approach in treating internal rotation was similar in principle to previously reported methods.[29,34] First, the hindrance potential energy surface (PES) for each rotation about polyvalent single bonds was obtained by scanning the dihedral angle in 30° increments. The dihedral angle was fixed and the rest of the structure was allowed to relax with the geometry optimized using the B3LYP/6-31G(d) level of theory. Although rigid scans are more computationally efficient, significant errors were encountered due to the branching of the molecules under consideration. In particular, the peroxy radical and hydroperoxide moieties gave nonphysical PES results when the superstructure was kept rigid. Examples of this are provided in the Supporting Information. To preserve the structure of the reactive center during relaxed PES scans of transition states, all coordinates that constituted the ring of each transition state were frozen, while all other coordinates except the dihedral angle being scanned were optimized. Once the PES for each rotation was obtained, the one-dimensional Schrödinger equation was solved in order to obtain the energy levels for each rotation. This step was performed using the Fourier grid Hamiltonian (FGH) method developed by Marston and coworkers.[35,36] To obtain the correct energy levels, the numerical algorithm for the FGH method was implemented using published source code.[37] The energy levels from this calculation were used to calculate the partition function for each internal rotation as a function of temperature:

$$Q_{ir} = \frac{1}{\sigma_r}\sum_i g_i \exp\left(-\frac{\epsilon_i}{kT}\right) \qquad (1)$$

where σ_r is the internal symmetry number of the rotating top and g_i is the degeneracy of the ith energy level, ϵ_i.[29]

In making the correction to the HO partition function, the vibrational modes corresponding to internal rotation must be identified and their contribution to the HO partition function removed.[34,38] For each vibration, the contributions from various bonds, angles, and dihedrals were analyzed using the internal mode analysis provided by Gaussian 03. In large molecules, there is often substantial mixing of vibrational modes resulting in a number of low frequencies corresponding to multiple different internal rotations. Potential problems arising from this mixing of vibrational modes have recently been outlined.[39] Our present approach is to use the internal mode analysis to identify a single low-frequency vibration for each internal rotation in a given molecule. Thus, the HO partition function for a molecule with n dihedral angles was corrected by (i) removing the contribution of n low-frequency vibrational modes and (ii) including the contribution of n internal rotations.

Once the partition functions for each reactant and transition state were corrected for internal rotation, the rate constant as a function of temperature was calculated using the standard expression,

$$k_{TST} = rpd^*\kappa(T)\frac{k_b T}{h}\frac{Q^{\ddagger}(T)}{Q^r(T)}\exp(-E_o/RT) \qquad (2)$$

where *rpd* is the reaction path degeneracy, determined by the number of identical hydrogen atoms a particular radical can self-abstract, $Q^{\ddagger}$ and Q^r are the total partition functions for the TS and reactant, respectively, and E_o is the reaction barrier, i.e., the zero-point corrected difference between the ground-state electronic energies of the TS and the reactant. The quantity $\kappa(T)$ is the correction for quantum tunneling. To quantify the effect of quantum tunneling on the reactions of interest here, we calculated various approximations to the transmission coefficient including the Wigner[40] correction, the Eckart approximation,[41] the zero-curvature approximation (ZCT),[41] and the small curvature tunneling (SCT)[41] approximation. Calculation of the Eckart, SCT, and ZCT corrections was performed using the software package "Virtual Kinetic Laboratory" of Zhang and Truong.[42] Once the temperature-dependent partition functions were known, rate constants as a function of temperature were calculated, and the Arrhenius parameters A and E_a were obtained from a straight-line fit of ln k vs $1/T$. Unless otherwise stated, we used a temperature range of 300−1000 K for regression of A and E_a. To calculate the enthalpy of reaction, all thermodynamic parameters were obtained from ensemble energy averages $\langle E\rangle$ using standard formulas.[32]

Thermochemistry of Peroxide Species. Although the B3LYP functional has been repeatedly shown to give accurate results for the heat of reaction and heat of formation, especially when compared to other methods of similar computational cost, it has been documented that B3LYP systematically gives errors in the bond dissociation energy of the O−O and O−H bonds in hydroperoxide moieties.[3,43] The standard approach is to use isodesmic reactions to obtain a corrected heat of formation.[44] Although this correction for reactants and products is straightforward, an analogous treatment for the TS is not obvious. Therefore, the heats of reaction reported are the difference in the quantum chemical enthalpies between the reactant and product species, which offered a method that was consistent with the manner in which the activation energy was calculated for the structure/reactivity relationships that were developed.

Treatment of Rotational Isomers. It was observed that in some cases the IRC-derived reactants were not the minimum energy structures. Subsequent rotation of the C−O bond in the peroxy radical or rotation about the backbone of the molecule could yield a reactant lower in energy typically by no more than 1 kcal mol^{-1}. While these were relatively subtle differences, it was still important to account for them in the evaluation of

methods and development of the structure/reactivity relationships. For reactants in which a lower energy structure was found, the following modified rate constant was used:

$$k_{\text{apparent}} = K_{\text{eq}}^{\text{rot}}(T)*k_{\text{TST}}(T) \quad (3)$$

where $K_{\text{eq}}^{\text{rot}}$ is the equilibrium constant between two rotational isomers:

$$K_{\text{eq}}^{\text{rot}} = e^{-\Delta G^{\text{rot}}(T)/RT} \quad (4)$$

Thus, the activation energy and pre-exponential factor were regressed from a fit of $\ln(k_{\text{apparent}})$ versus $1/T$. A full derivation of this relationship is provided in the Supporting Information.

3. Results and Discussion

Effect of Basis Set on Results Obtained from the B3LYP Functional. Results for the comparison of 16 different methods and the 3 different reactions studied in detail (reactions 1−3 in Figure 1) are listed in Table 1. The first 11 entries in each section of the table list B3LYP calculations performed with increasingly larger basis sets. The one non-Pople basis set used was listed as the last of these 11 for clarity. The bottom five lines in each section of Table 1 contain results for these reactions with different MO, DFT, and hybrid methods. The results show that the choice of the basis set has a strong impact on both the reaction barrier and the heat of reaction. As expected, increasing the size of the basis set generally improves the agreement between the B3LYP results and experimental data or results from the high-level compound methods. With one exception in which the calculated activation energy was equal to the experimental value, all of the B3LYP methods overestimate the experimental activation energies. This corresponds to an underprediction of the reaction rate coefficient. One possible explanation for this could be the type of calculation used to estimate the contribution of quantum tunneling, but our results show that the type of tunneling correction used did not change the calculated activation energies significantly. We calculated the Eckart, ZCT, and SCT transmission coefficients for reactions 1 and 2 using the B3LYP/6-31G(d) and B3LYP/6-311+G(d,p) basis sets. The Wigner correction was a good approximation of the SCT transmission coefficient (within a factor of 2 or less at the temperature range of interest (373 K)). Accordingly, we calculated all kinetic data in Table 1 using the Wigner correction. Furthermore, the transmission coefficient had a maximum value of 3.7 at 300 K for the reactions we studied, which is much lower than that observed for intermolecular hydrogen transfer reactions of small molecules studied by Truong and co-workers[45] and Gonzalez-Lafont and co-workers.[41] The small contribution of tunneling is consistent with the adiabatic ground state potential clearly showing a *very* late transition state. The potential is nearly flat as the reaction goes from the transition state to the product hydroperoxide radical (forward direction as depicted in Figure 1). Because tunneling is not observed to have a strong impact in these reactions, it is not surprising that for each reaction in Table 1, a plot of ln k versus $1/T$ gave a perfect straight-line fit, thereby validating our method of obtaining the Arrhenius parameters A and E_a.

Because we are seeking kinetic correlations for use in condensed-phase hydrocarbon oxidation chemistry, we tested the sensitivity of the calculated data to the presence of a nonpolar solvent, i.e., a typical oxidation substrate of interest. We used the PCM model to simulate a solvent cavity of *n*-heptane and reoptimized the reactants, TS, and products for reactions 1−3 using B3LYP/6-31G(d). As shown in Table 1, the PCM model does not result in any appreciable change in the calculated kinetic properties or enthalpy of reaction. This agreement between gas-phase TST calculations and condensed-phase kinetic data has also been observed for other reaction classes.[46] However, it is important to note the rate of hydrogen abstraction in the condensed phase has also been shown to be a strong function of the polarity of the solvent.[47]

These results add to the growing database of activation energies predicted by B3LYP, which collectively suggests that B3LYP does not exclusively under- or overestimate reaction barriers. Furthermore, it is not generally possible a priori to state in which direction B3LYP will err. For example, Wijaya and co-workers[3] report an underestimation by B3LYP of the barrier height for different cyclization reactions while Henry and Radom[46] report that B3LYP always overpredicts the barrier for the cyclization of but-3-enyl-radical. The heats of reaction are not available from experiment, but two observations can be drawn based on the results provided. First, results from very small basis sets deviate strongly from the CBS and G3 methods, with errors as large as 4 kcal mol^{-1}. Moving to very large basis sets improves the agreement with the CBS and G3 results, with some B3LYP heats of reaction higher than the CBS-QB3 values by only 1 kcal mol^{-1}. Finally, it is worthwhile to note that the barriers calculated using B3LYP/6-311+G(3df,2p) differ from those calculated using single point calculations from the same method but with geometries optimized using B3LYP/6-31G(d). Using the smallest basis set (6-31G(d)) for geometry optimization and the largest basis set (6-311+G(3df,2p)) for single point calculations gives activation energies that may deviate significantly from the experimental, CBS, and G3 results.

It is next interesting to compare the five higher level methods in the bottom of each section of Table 1 with each other. Barriers calculated at the MP2 and G3(MP2) levels of theory are in very poor agreement with the experimental data for all three reactions. To test if the cause of this discrepancy was from the optimized geometries or from the single point/hybrid energies, we calculated the G3//B3LYP energy of the reactant and TS of the MP2/6-311+G(d,p) optimized structures for reaction 2. The calculated activation energy was nearly identical to the full G3//B3LYP activation energy, thus indicating that the energies calculated using MP2 are poor. The BHandHLYP/6-311G(d,p) method also substantially overpredicts the activation barrier compared to the CBS-QB3 method. Despite their poor predictions of the barrier height, BHandHLYP/6-311G(d,p), MP2/6-311+G(d,p), and G3(MP2) still give pre-exponential values that are in good agreement with the value obtained from CBS-QB3, and the heats of reaction are in reasonable agreement with the B3LYP values using large basis sets. In comparing the two hybrid methods, the results reveal that in the case of the first and second reactions, CBS-QB3 gives results that are much closer to the experimentally reported values, whereas the experimental values for the third reaction more closely match the G3B3 results. However, each activation energy was obtained from a single source without any repeatability reported. Therefore, the comparison set is too limited to draw any definitive conclusion about the superiority of either of these methods. Additionally, in all cases, the calculated rate coefficients ($k_{\text{TST}}(373\ K)$) from the CBS-QB3 method give the best agreement to the available experimental data. For calculating rate coefficients, the G3//B3LYP method performs noticeably better than pure B3LYP methods for reaction three, but at a comparable (or lower) level of accuracy for reactions 1 and 2. For example, in the data set for reaction 1, B3LYP/cc-pVTZ+d

TABLE 1: Comparison of Basis Set and Method for Three Intramolecular Hydrogen Abstraction (Reactions 1−3 in Figure 1)

						reactants		transition state		
method[a]	E_o[b]	ΔH_{rxn}[c]	E_a[d]	log A[e]	k_{TST}(373 K)[f]	ν_{ir}[g]	$\langle S^2\rangle$[h]	ν_{ir}[g]	ν_i[i]	$\langle S^2\rangle$[h]
reaction 1[j]					$C(CH_3)_2(O_2^{\bullet})CH_2CH(CH_3)_2 \rightarrow C(CH_3)_2(O_2H)CH_2C^{\bullet}(CH_3)_2$					
6-31G(d)	19.8	17.8	21.1	10.8	2.73×10^{-2}	47,75,110,181,207,229,242	0.753	193,201,205,225	−1626	0.756
6-31G(d)[k]	19.4	17.2	20.6	10.7	4.26×10^{-2}					
RO 6-31G(d)[l]	20.0	17.7	21.2	10.8	2.38×10^{-2}	47,75,111,181,207,229,242		194,201,205,225	−1695	
6-31G(d,p)	18.0	15.5	19.2	10.8	3.54×10^{-1}	48,76,111,180,209,219,243	0.753	195,200,206,226	−1610	0.756
6-311G(d,p)	17.7	14.3	19.0	10.7	3.69×10^{-1}	47,76,111,178,202,215,243	0.754	194,197,206,227	−1653	0.756
6-311+G(d,p)	17.7	13.7	18.7	10.6	4.39×10^{-1}	48,75,103,178,208,228,242	0.754	193,200,205,227	−1654	0.756
RO 6-311+G(d,p)[l]	17.8	13.6	18.8	10.6	3.83×10^{-1}	48,75,104,178,208,228,242		194,200,205,227	−1713	
6-311+G(df)	20.2	16.7	21.3	10.7	1.65×10^{-2}	55,77,99,178,213,220,245	0.754	194,203,206,228	−1694	0.757
6-311+G(3df,2p)	17.4	13.4	18.5	10.7	7.24×10^{-1}	47,72,101,177,208,228,242	0.755	192,199,204,226	−1675	0.757
6-311+G(3df,2p)[m]	16.6	13.4	19.1	10.8	4.05×10^{-1}	47,75,110,181,207,229,242	0.753	193,201,205,225	−1626	0.753
cc-pVTZ+d	17.4	13.6	18.5	10.7	7.24×10^{-1}	44,74,106,178,204,227,240	0.754	194,196,204,226	−1666	0.756
MP2/6-311+G(d,p)[e]	34.1	17.7	35.7	10.6	4.79×10^{-11}	60,66,93,180,221,232,259	0.763	208,215,228,252	−2033	0.794
BHandHLYP/6-311G(d,p)	23.4	14.7	24.7	10.7	1.68×10^{-4}	51,76,119,187,217,234,256	0.757	206,210,219,242	−2133	0.765
G3(MP2)	43.7	13.7	44.8	10.9	4.45×10^{-16}	48,71,124,193,241,252,267	0.761	262,302,315,336	−2777	0.797
G3\\B3LYP	17.9	12.9	19.2	10.8	3.54×10^{-1}	47,75,110,181,207,229,242	0.753	193,201,205,225	−1626	0.756
CBS-QB3	16.3	12.3	17.5	10.6	2.22	44,79,111,178,200,219,244	0.754	185,202,215,238	−1653	0.756
experimental			17.5	11.5	18					
reaction 2					$CH_3C(O_2^{\bullet})H(CH_2)_2CH_3 \rightarrow CH_3C(O_2H)HCH_2C^{\bullet}HCH_3$					
6-31G(d)	24.0	19.6	23.1	10.9	2.31×10^{-3}	71,79,108,169,206	0.753	193,210	−1628	0.757
6-31G(d)[k]	23.5	19.1	22.5	10.8	4.13×10^{-3}					
RO 6-31G(d)[l]	24.9	20.2	23.9	10.8	6.24×10^{-4}	78,86,107,176,241		187,208	−1711	
6-31G(d,p)	22.7	17.9	21.7	10.8	1.21×10^{-2}	73,84,106,176,234	0.753	189,206	−1637	0.756
6-311G(d,p)	22.5	16.8	21.5	10.8	1.59×10^{-2}	77,82,104,176,232	0.753	189,197	−1682	0.756
6-311+G(d,p)	22.3	16.3	21.3	10.8	2.08×10^{-2}	71,79,108,176,230	0.754	190,203	−1690	0.757
RO 6-311+G(d,p)[l]	22.5	16.0	21.5	10.8	1.59×10^{-2}	71,81,108,176,230		191,203	−1753	
6-311+G(df)	25.1	19.2	24.1	10.8	4.76×10^{-4}	68,78,104,176,231	0.754	191,206	−1726	0.757
6-311+G(3df,2p)	22.1	15.8	21.1	10.8	2.73×10^{-2}	72,80,109,176,227	0.755	187,202	−1716	0.757
6-311+G(3df,2p)[m]	20.6		19.7	10.9	2.27×10^{-1}	71,79,108,169,206	0.753	193,210	−1628	0.757
cc-pVTZ+d	21.3	15.3	20.4	10.8	7.02×10^{-2}	39,76,106,167,200	0.754	188,201	−1703	0.757
MP2/6-311+G(d,p)[n]	40.6	19.3	39.4	10.7	4.10×10^{-13}	67,73,109,175,242	0.763	213,215	−2098	0.796
BHandHLYP/6-311G(d,p)	27.6	16.0	26.3	10.8	2.45×10^{-5}	54,80,112,171,214	0.756	202,211	−2190	0.765
G3(MP2)	40.9	15.3	38.9	9.9	1.28×10^{-13}	73,87,117,179,237	0.761	124,163	−2979	0.800
G3\\B3LYP	21.7	14.7	20.8	10.9	5.15×10^{-2}	71,79,108,169,206	0.753	193,210	−1628	0.757
CBS-QB3	20.2	14.4	19.3	10.9	3.90×10^{-1}	47,77,107,167,202	0.754	189,197	−1682	0.756
experimental			19.7	11.5	8.7×10^{-1}					
reaction 3[j]					$C(CH_3)_2(O_2^{\bullet})(CH_2)_2CH(CH_3)_2 \rightarrow C(CH_3)_2(O_2H)(CH_2)_2C^{\bullet}(CH_3)_2$					
6-31G(d)	20.0	16.6	19.9	9.4	5.48×10^{-3}	49,79,99,139,198,207,230,230	0.753	197,204,219,230	−1628	0.757
6-31G(d)[k]	19.7	16.2	19.6	9.4	8.22×10^{-3}					
RO 6-31G(d)[l]	20.3	16.4	20.1	9.4	4.19×10^{-3}	49,79,99,140,198,207,230,231		198,204,220,231	−1758	
6-31G(d,p)	18.3	14.3	18.0	9.4	7.12×10^{-2}	50,80,100,141,197,209,230,231	0.753	199,205,219,231	−1654	0.756
6-311G(d,p)	17.9	13.1	17.7	9.3	8.48×10^{-2}	50,81,100,143,193,207,225,229	0.754	197,206,216,232	−1695	0.757
6-311+G(d,p)	17.8	13.1	18.0	9.3	5.66×10^{-2}	49,76,95,138,198,209,226,228	0.754	196,207,218,232	−1702	0.757
RO 6-311+G(d,p)[l]	17.9	12.8	18.1	9.3	4.94×10^{-2}	49,76,95,138,199,208,226,229		196,207,218,232	−1773	
6-311+G(df)	20.2	16.0	20.4	9.3	2.22×10^{-3}	51,72,96,140,201,211,227,232	0.754	196,207,220,232	−1740	0.757
6-311+G(3df,2p)	17.7	12.8	18.0	9.3	5.66×10^{-2}	46,72,92,133,198,206,226,228	0.755	194,205,216,231	−1730	0.757
6-311+G(3df,2p)[m]	16.7		19.3	9.4	1.23×10^{-2}	49,79,99,139,198,207,230,230	0.753	197,204,219,230	−1675	0.757
cc-pVTZ+d	17.8	12.9	18.0	9.3	5.66×10^{-2}	46,75,95,137,196,206,226,227	0.754	195,204,215,231	−1721	0.757
MP2/6-311+G(d,p)[n]	34.2	18.4	34.9	9.3	7.07×10^{-12}	60,86,108,143,203,223,228,242	0.763	213,223,227,238	−2164	0.794
BHandHLYP	23.4	13.7	23.0	9.2	5.28×10^{-5}	50,85,106,149,206,218,233,241	0.757	210,220,223,239	−2214	0.765
G3(MP2)	47.0	12.0	44.7	7.5	2.03×10^{-19}	43,79,103,153,217,239,246,257	0.761	83,95,198,254	−2875	0.797
G3\\B3LYP	17.9	10.6	16.7	9.4	4.11×10^{-1}	49,79,99,139,198,207,230,230	0.753	197,204,219,230	−1675	0.757
CBS-QB3	16.5	10.6	15.9	9.3	9.62×10^{-1}	50,81,100,144,194,208,226,229	0.754	197,206,216,232	−1695	0.757
experimental			17.2	11	8					

[a] Unless alternate MO or hybrid method is given, the B3LYP functional is used and only the basis set is provided. [b] Reaction barrier (in kcal/mol). [c] Heat of reaction (in kcal/mol) at 298 K. [d] Arrhenius activation energy (in kcal/mol). [e] Pre-exponential factor (in 1/s). [f] Rate coefficient (in 1/s) at 373 K. [g] Frequencies (in cm^{-1}, unscaled) which were identified as hindered rotors. [h] Expectation value of the total spin for the reactants and the transition states. [i] Imaginary vibrational mode (in cm^{-1}) of the transition state. [j] Lower energy rotational isomer of IRC-derived reactant or product was found, and eq 3 was used to calculate the pre-exponential factor and activation energy for the forward reaction. [k] Geometry optimization and energy calculation performed using UB3LYP/6-31G(d) and a PCM model using the properties of *n*-heptane to describe the solvent cavity. [l] Calculation performed with restricted-open shell wavefunctions. [m] Geometry optimization performed at UB3LYP/6-31G(d) with single point and frequency calculation at given basis set. [n] MP2 scaling factors of 0.9670 (ZPE) and 0.9434 (fundamental frequencies) were used according to the recommendation of Scott and Radom.[28]

gives a rate coefficient of 7.24×10^{-1} (1/s), whereas the prediction of G3//B3LYP is 3.54×10^{-1} (1/s). Both calculations are far from the single experimental value of 18 (1/s), but the cc-pVTZ+d value is a factor of 2 closer.

Given the variability of the results from all of the different methods and basis sets, it is instructive to compare their computational cost. Figure 2 gives the relative computational cost for B3LYP using the 6-31G(d), 6-311+G(d,p), 6-311+G(3df,2p), and cc-pVTZ+d basis sets, as well as CBS-QB3 and G3//B3LYP for the reactants of reactions 2 and 3 in Figure 1. The largest basis sets that most closely approximate the hybrid methods cost slightly more than the CBS-QB3 calculation, whereas G3//B3LYP is noticeably more expensive than the other methods. The high computational cost of G3//B3LYP is due almost entirely to the single point calculation using the MP4/6-31G(2df,p) level of theory. On the basis of the relatively good performance of the B3LYP/6-311+G(d,p) calculations on all three reactions and its modest computational cost, we selected

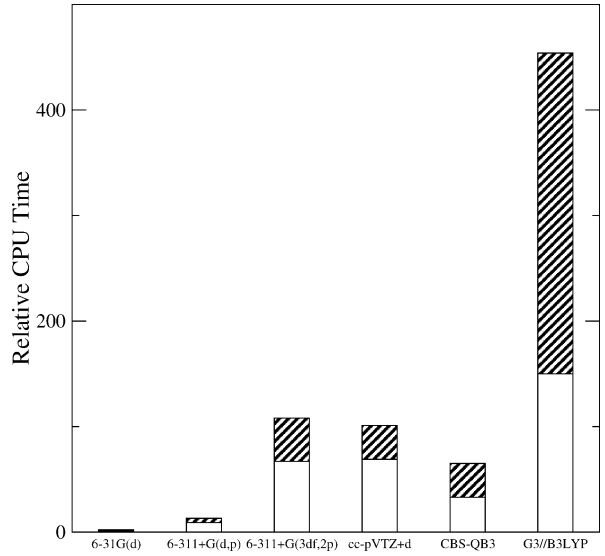

Figure 2. Comparison of computational cost for the B3LYP functional with several basis sets and two hybrid methods. Two reactants are compared: $CH_3C(O_2^{\bullet})HC_3H_7$ (white bars) and $C(CH_3)_2(O_2^{\bullet})(CH_2)_2CH(CH_3)_2$ (striped bars). All times are relative to the B3LYP/6-31G(d) calculation of $CH_3C(O_2^{\bullet})HC_3H_7$.

this basis set to study other substituent and structural effects in this reaction family. Our performance criterion was based on the ability of a given method to accurately calculate the activation energy. This is based on an approach for estimating reaction rate coefficients that is often applied to large reaction mechanisms that consist of thousands of reactions in which a representative frequency factor is assumed for all reactions in a given reaction family and the activation energy for individual reactions is calculated using structure−reactivity relationships based on thermodynamic properties.[8,48,49] Although CBS-QB3 would be the best choice based on agreement of the calculated rate coefficients with experimental data, a full exploration of substrate size and substituent effects is not feasible using such an expensive hybrid method due to the large number of reactions proposed for study in Figure 1 as well as the poor scaling of hybrid methods. Therefore, we selected B3LYP/6-311+G(d,p) as a good compromise between cost and accuracy for calculating activation energies. Combining the calculated activation energies with a representative frequency factor based on experimental data would yield values of rate coefficients in very good agreement with experiment.

Effect of Ring Size. To probe the effect on the rate coefficient for this class of reactions of the relative position from which the hydrogen was abstracted, we varied the ring size of the transition state from four to seven. The four-membered ring corresponds to a 1,3-hydrogen shift and the seven-membered ring results from a 1,6-hydrogen shift. The degree of substitution of the carbon atoms attached to the reacting hydrogen and to the $OO^{\bullet}$ moiety was the same for all four reactions so that rate constants could be compared fairly. The four reactions examined are reactions 1, 3, 10, and 11 in Figure 1. The activation energies and pre-exponential factors are summarized in Table 2. The relationship between ring size and activation energy is a decreasing, nonlinear function as seen in Figure 3. The decrease in the activation energy is particularly marked beyond a ring size of six as the ring strain becomes minimized. As the ring size of the TS is increased, an additional internal rotation is lost or frozen within the TS ring structure. Thus, the partition function for the reactant increases more than the partition function for the TS as the ring size is increased, causing the pre-exponential factor to decrease with increasing ring size. The proportional decrease in the pre-exponential factor with increasing ring size is clearly seen in the plot of the pre-exponential factor as a function of ring size in Figure 3. Although the correlation is empirical, it can be explained based on changes in internal rotations, and the straight line behavior of the pre-exponential factor as a function of ring size may offer a simple template for the development of structure−reactivity relationships for systems in which intramolecular hydrogen transfer plays an important role.

A Simple Structure−Reactivity Relationship to Describe 1,5- Intramolecular Hydrogen Transfer. For reactions in the 1,5-hydrogen shift family, structural changes were introduced via substitution of various groups and atoms along the backbone to create diversity in thermodynamic and kinetic parameters of the reaction as delineated by reactions 1−2 and 4−9 in Figure 1. Starting with a very small substrate (reaction 6), we systematically introduced additional substitutions both near the hydrogen undergoing abstraction as well as the peroxy radical moiety. This approach ensured that a broad range of heats of reaction was explored, thus creating a more general structure−reactivity relationship. It is interesting to note that even though almost all degrees of substitution were explored, there were no forward reactions with a heat of reaction less than 8.5 kcal mol^{-1}. In addition, we investigated the effect of introducing structural changes to the TS ring by adding a carbonyl linkage to reactions 6, 2, and 5 to create carbonyl-containing reactants in reactions 7−9, respectively. Thermodynamic and kinetic data for 16 reactions (forward and reverse pairs) considered are summarized in Table 3, and the heats of reaction and activation energy data in Table 3 are plotted in Figure 4. Also included in Table 3 are data for reaction 8 calculated using CBS-QB3.

For the forward reactions, the first five reactions listed in Table 3 fall on an Evans−Polanyí[7] correlation, i.e., $E_a = E_o + \alpha\Delta H_{rxn}$. The parameters regressed from these data are $E_o =$ 6.3 kcal mol^{-1} and $\alpha = 1$. The regressed transfer coefficient indicates that this reaction family is more sensitive to the influence of substituents than intermolecular hydrogen transfer, which is often approximated with a transfer coefficient of 0.8.[6] In this case, the approximated activation energy is the heat of reaction added to the intrinsic reaction barrier. The best fit for the activation energy of the reverse reactions as a function of heat of reaction is a straight line with a slope equal to zero and an intercept equal to the intrinsic reaction barrier for the forward reactions of 6.3 kcal mol^{-1}. This enthalpic consistency is clarified by examining the relationship $E_a = \Delta H^{\ddagger} + nRT$ from transition state theory, where n is the molecularity of the reaction. When manipulated algebraically, this equation reveals that for forward and reverse reaction pairs of reactions in the intramolecular hydrogen transfer reaction family, the sum of the transfer coefficients is equal to 1, and the intrinsic barriers are equal, as observed here. In the practice of creating detailed kinetic models, overall thermodynamic consistency would be enforced by using only one of the two Evans−Polanyí relationships to calculate the rate coefficient in one direction while the other would be calculated based on a known equilibrium constant. However, the two distinct Evans−Polanyí relationships are clearly enthalpically consistent within the approximation of $E_a = \Delta H^{\ddagger} + nRT$, and thus, each relationship may be used independently to estimate the activation energy depending on the specific type of reaction of interest. A transfer coefficient of one is also known to correspond to a very late transition state that is consistent with the IRCs calculated.

TABLE 2: Comparison of Activation Energy and Pre-Exponential Factor as the Ring Size of the Transition State Is Varied from 4 to 7[a]

reaction	TS ring size	E_a[b]	log *A* (1/s)
$CH_3CH(O_2^{\bullet})CH_3 \rightarrow CH_3COCH_3 + HO^{\bullet}$ [c]	4	41.6	12.6
$(CH_3)_2C(O_2^{\bullet})CH(CH_3)_2 \rightarrow (CH_3)_2C(O_2H)C^{\bullet}(CH_3)_2$	5	28.0	11.5
$C(CH_3)_2(O_2^{\bullet})CH_2CH(CH_3)_2 \rightarrow C(CH_3)_2(O_2H)CH_2C^{\bullet}(CH_3)_2$	6	18.7	10.6
$C(CH_3)_2(O_2^{\bullet})(CH_2)_2CH(CH_3)_2 \rightarrow C(CH_3)_2(O_2H)(CH_2)_2C^{\bullet}(CH_3)_2$	7	18.0	9.3

[a] Geometry optimization and energy calculations were performed using B3LYP/6-311+G(d,p). [b] Quantity in kcal mol^{-1}. [c] The 1,3-hydrogen shift creates the unstable $^{\bullet}$COOH containing radical, which directly yields the β-scission products shown in the table.

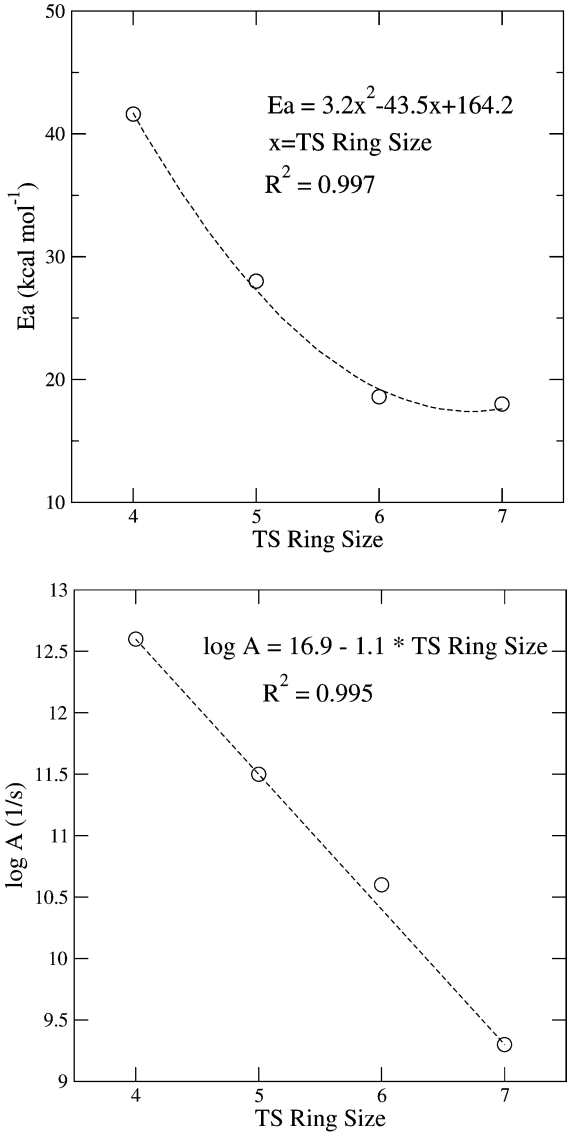

Figure 3. Variation of Arrhenius activation energy and pre-exponential factor with transition state ring size. A regression line is given to show the variation of each parameter as the ring size is increased.

Blowers and Masel[6] have proposed a modified form of the Marcus equation to estimate the activation energy of hydrogen transfer reactions for endo- and exothermic reactions using a single formulation as shown in eq 5.

$$E_a = \begin{cases} 0 & \text{for } \Delta H_{rxn}/4E_o < -1 \\ E_o(1 + \Delta H_{rxn}/4E_o)^2 & \text{for } -1 \le \Delta H_{rxn}/4E_o \le 1 \\ \Delta H_{rxn} & \text{for } \Delta H_{rxn}/4E_o > 1 \end{cases} \quad (5)$$

Their proposed relationship is second order in the heat of reaction and nicely captures the curved transition region between exothermic and endothermic reactions in bimolecular hydrogen transfer reactions. We varied E_o to fit our data to the Blowers−Masel relationship, but the fit was very poor due to the inability of the Blowers−Masel relationship to asymptotically approach a nonzero value for strongly exothermic reactions. A modified Blowers−Masel relationship in which a constant was added to the equation for each regime in eq 5 fit the data well with a value of $E_o = 3.7$ kcal mol^{-1} and a constant factor of 6.2 kcal mol^{-1}. This suggests that the intrinsic barrier for strongly exothermic reactions approaches a value of 6.2 kcal mol^{-1} instead of zero for this class of reactions. However, because of the lack of data in the endo- to exothermic transition region, it is not possible to estimate whether the Blowers-Masel relationship is superior to the simple Evans−Polanyí relationship.

Reactions 7−9 are also plotted in Figure 4 and clearly fall on a different correlation than the corresponding reactants without carbonyl groups. The calculation for reaction 8 was repeated using CBS-QB3 to verify that higher-level methods also capture this difference. The data in Table 3 show that B3LYP/6-311+G(d,p) and CBS-QB3 are in very good agreement. Linear regression shows that the data for reactants containing a carbonyl linkage in the TS ring have a different Evans−Polanyí relationship. The intrinsic barrier, E_o, is 18.1 kcal mol^{-1} and the endothermic/exothermic transfer coefficients, α, are 0.74 and 0.26, respectively. Although these transfer coefficients are much more similar to typical hydrogen transfer values, the intrinsic barrier is much larger than typical hydrogen transfer values of 7−10 kcal mol^{-1}. One possible explanation for this is increased ring strain due to the carbonyl linkage. Also, in the product structure, the carbonyl group offers significant stabilization to the radical center on the adjacent carbon atom, resulting in a heat of reaction that is much lower than the alkyl counterpart. We also explored the effect of tunneling on this reaction class given the distinct structure−reactivity relationship and the markedly different heats of reaction compared to the analogous reactions without the intervening carbonyl group. For all three reactions, we calculated the SCT, ZCT and Eckart transmission coefficients as a function of temperature. The Eckart model was observed to significantly overestimate the SCT values in the low temperature region. Conversely, the ZCT and Wigner transmission values were noticeably lower than the SCT values. Using eq 2 with the transmission coefficient based on the SCT method, we recalculated the activation energies using rate constants over a small temperature range (300−600 K). The SCT/TST activation energies were lower than the corresponding Wigner/TST activation energies with the deviation between the two methods ($E_a^{Wigner} - E_a^{SCT}$) ranging between 1.6 and 2.8 kcal mol $^{-1}$; however, the same form of structure−reactivity relationship was observed, with E_o and α values of 15.6 kcal mol $^{-1}$ and 0.83/0.17.

4. Conclusions

The B3LYP functional was evaluated as a method to calculate reaction barriers and structure−reactivity relationships for intramolecular hydrogen transfer reactions involving peroxy

TABLE 3: Data Used in Development of Structure−Reactivity Relationship for 1,5-Hydrogen Shift Family[a]

		forward reaction			reverse reaction	
number	reaction	ΔH_{rxn} [b]	E_a [b]	log A (1/s)	Ea[b]	log A (1/s)
1	$C(CH_3)_2(O_2^{\bullet})CH_2CH(CH_3)_2 \rightarrow C(CH_3)_2(O_2H)CH_2C^{\bullet}(CH_3)_2$ [c]	13.7	18.7	10.6	5.1	9.7
2	$CH_3C(O_2^{\bullet})H(CH_2)_2CH_3 \rightarrow CH_3C(O_2H)HCH_2C^{\bullet}HCH_3$	16.3	21.3	10.8	5.8	10.7
4	$(CH_3)_2CHCH_2C(O_2^{\bullet})(CH_3)CH_2CH(CH_3)_2 \rightarrow (CH_3)_2C^{\bullet}CH_2C(O_2H)(CH_3)CH_2CH(CH_3)_2$	8.6	16.8	11.3	6.1	11.1
5	$(CH_3)CH(O_2^{\bullet})CH_2CH(CH_3)_2 \rightarrow (CH_3)CH(O_2H)CH_2C^{\bullet}(CH_3)_2$ [c]	14.9	21.6	10.6	8.0	10.9
6	$(CH_3)CH(O_2^{\bullet})CH_2CH_3 \rightarrow (CH_3)CH(O_2H)CH_2C^{\bullet}H_2$ [c]	19.6	26.2	11.2	7.1	11.6
7	$(CH_3)CH(O_2^{\bullet})COCH_3 \rightarrow (CH_3)CH(O_2H)COC^{\bullet}H_2$	11.6	26.3	11.1	15.3	12.5
8	$(CH_3CH(O_2^{\bullet})HCOCH_2CH_3 \rightarrow (CH_3CH(O_2H)HCOCH^{\bullet}CH_3$	4.0	21.3	11.6	17.6	12.0
8	$(CH_3CH(O_2^{\bullet})HCOCH_2CH_3 \rightarrow (CH_3CH(O_2H)HCOCH^{\bullet}CH_3$ [d,e]	2.7	20.8	11.7	17.8	11.0
9	$(CH_3)CH(O_2^{\bullet})COCH(CH_3)_2 \rightarrow (CH_3)CH(O_2H)COC^{\bullet}(CH_3)_2$	1.5	19.1	10.4	17.4	10.1

[a] When applicable, lower energy rotational isomers were used, according to eq 3. Unless noted, all calculations were performed using B3LYP/6-311+G(d,p) [b] Quantity in kcal mol^{-1}. [c] Lower energy rotational isomer of IRC-derived reactant was found and eq 3 was used to calculate the pre-exponential factor and activation energy for the forward reaction. [d] Value not used in regression of structure/reactivity relationship. [e] Reaction thermodynamics and kinetics calculated using CBS-QB3.

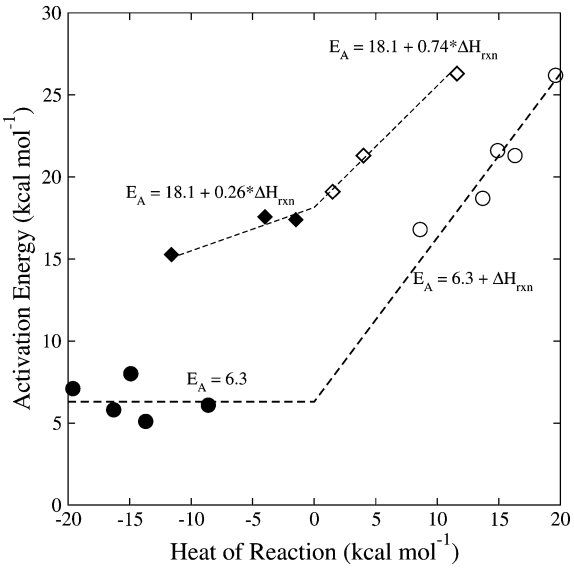

Figure 4. Plot of activation energy versus heat of reaction for all reactions studied in the 1,5-hydrogen shift family. All of the B3LYP/6-311+G(d,p) data from Table 3 are included in the figure, but two different regressions were performed to reflect the different relationships observed. The open and closed circles indicate all data that are forward/reverse reaction pairs of the alkylperoxy radicals (reactions 1−2 and 4−6 in Figure 1). The open and closed diamonds indicate the data that contain carbonyl moieties within the TS ring structure (reactions 7−9 in Figure 1). The recommended structure−reactivity relationships are given within the figure with units of kcal mol^{-1}.

radicals. Nine different basis sets as well as five other MO/DFT and hybrid methods were used in comparing three reactions to available experimental data. It was shown that B3LYP/6-311+G(d,p) offers a good compromise between speed and accuracy for studies in which thermodynamic and kinetic data of many reactions are required. The BHandHLYP functional and methods based on MP2 geometries gave very poor predictions of experimental activation energies, and their reaction barriers disagreed substantially from those obtained with CBS-QB3 and G3//B3LYP, whose applicability has been extensively tested.

We probed the effect of varying the transition state ring size as well as the effect of substituent groups for the 1,5-hydrogen shift family. Clear trends were observed when the ring size was varied and all other substituents were held constant. As expected, increasing the ring size led to decreased activation barriers as well as decreasing pre-exponential factors. Evans−Polanyí relationships were shown to capture the activation energy as a function of heat of reaction for reactions in the 1,5-hydrogen shift family. A pre-exponential factor of log A (s^{-1}) = 10.9 and $E_a = 6.3 + \Delta H_{rxn}$, where E_a and ΔH_{rxn} are in kcal mol^{-1}, are recommended if there are no carbonyl groups in the transition state ring structure. Rate coefficients for reverse reactions in this family can be approximated using a pre-exponential factor of 10.8 (log A (s^{-1})) and an activation energy of 6.3 kcal mol^{-1}. If a carbonyl group within the ring structure was present, an Evans−Polanyí relationship $E_a = 18.1 + 0.74\Delta H_{rxn}$ ($\alpha = 0.26$ for exothermic reactions) was shown to capture the data well. The vast difference in the parameters of the two distinct correlations demonstrates that different structure−reactivity relationships are warranted. On the basis of the results obtained, B3LYP/6-311+G(d,p) is an attractive choice for obtaining insights into structure−reactivity relationships.

Acknowledgment. This work was partially supported by the NSF IGERT program (Award Number DGE-0114429) and the National Center for Supercomputing Applications under TG-CTS050021 utilizing the Pittsburgh Supercomputing Center. Support from the Inter-American Materials Collaboration Program of the National Science Foundation (DMR-0303435) is also acknowledged. We are grateful for helpful discussions with Peter Vansteenkiste and Dr. Veronique Van Speybroeck and also acknowledge the use of their code in calculating reduced moments of inertia and fitting rotational hindrance potentials.

Supporting Information Available: Comparison of rigid and relaxed PES scans for the C−O bond of a peroxy radical and a derivation of the apparent rate constant for combined rotational isomers and hydrogen transfer. This material is available free of charge via the Internet at http://pubs.acs.org.

References and Notes

(1) Blaine, S.; Savage, P. E. *Ind. Eng. Chem. Res.* **1992**, *31*, 69−75.
(2) Jensen, R.; Korcek, S.; Mahoney, L.; Zinbo, M. *J. Am. Chem. Soc.* **1981**, *103*, 1742−1749.
(3) Wijaya, C.; Sumathi, R.; Green, W. H., Jr. *J. Phys. Chem. A* **2003**, *107* (24), 4908−4920.
(4) Emanuel, N.; Gál, D. *Modelling of Oxidation Processes. Prototype: The Oxidation of Ethylbenzene*; Akadémiai Kiadoó: Budapest, 1986.
(5) Denisov, E. T.; Denisova, T. G. *Handbook of Antioxidants, Bond Dissociation Energies, Rate Constants, Activation Energies and Enthalpies of Reactions*; CRC Press: Boca Raton, 2000.
(6) Blowers, P.; Masel, R. I. *AIChE J.* **2000**, *46* (10), 2041−2052.
(7) Evans, M.; Polanyí, M. *Trans. Faraday Soc.* **1938**, *34*, 11−29.
(8) Boock, L. T.; Klein, M. T. *Ind. Eng. Chem. Res.* **1994**, *33* (11), 2554−2562.
(9) De Witt, M. J.; Dooling, D.; Broadbelt, L. J. *Ind. Eng. Chem. Res.* **2000**, *39* (7), 2228−2237.
(10) Kruse, T. M.; Wong, H.-W.; Broadbelt, L. J. *Macromolecules* **2003**, *36* (25), 9594−9607.

(11) Chan, W.; Hamilton, I.; Pritchard, H. *J. Chem. Soc., Faraday Trans.* **1998**, *94* (16), 2303−2306.
(12) Denisova, T. G.; Denisov, E. T. *Kinet. Catal.* **2001**, *42* (5), 620−630.
(13) Mill, T.; Hendry, D. In *Comprehensive Chemical Kinetics*; Elsevier: New York, 1980; Vol. 16, pp 2−87.
(14) Sickle, D. V.; Mill, T.; Mayo, F.; Richardson, H.; Gould, C. *J. Org. Chem.* **1973**, *38* (26), 4435−4440.
(15) Mill, T.; Montosori, G. *Int. J. Chem. Kinet.* **1973**, *5*, 119−136.
(16) Rust, F. *J. Am. Chem. Soc.* **1957**, *79* (15), 4000−4003.
(17) Merle, J. K.; Hayes, C.; Zalyubovsky, S.; Glover, B.; Miller, T.; Hadad, C. *J. Phys. Chem. A* **2005**, *109* (16), 3637−3646.
(18) Gomez-Balderas, R.; Coote, M. L.; Hendry, D.; Radom, L. *J. Phys. Chem. A* **2004**, *108* (15), 2874−2883.
(19) Frisch, M. J.; Trucks, G. W.; Schlegel, H. B.; Scuseria, G. E.; Robb, M. A.; Cheeseman, J. R.; Montgomery, J. A., Jr.; Vreven, T.; Kudin, K. N.; Burant, J. C.; Millam, J. M.; Iyengar, S. S.; Tomasi, J.; Barone, V.; Mennucci, B.; Cossi, M.; Scalmani, G.; Rega, N.; Petersson, G. A.; Nakatsuji, H.; Hada, M.; Ehara, M.; Toyota, K.; Fukuda, R.; Hasegawa, J.; Ishida, M.; Nakajima, T.; Honda, Y.; Kitao, O.; Nakai, H.; Klene, M.; Li, X.; Knox, J. E.; Hratchian, H. P.; Cross, J. B.; Bakken, V.; Adamo, C.; Jaramillo, J.; Gomperts, R.; Stratmann, R. E.; Yazyev, O.; Austin, A. J.; Cammi, R.; Pomelli, C.; Ochterski, J. W.; Ayala, P. Y.; Morokuma, K.; Voth, G. A.; Salvador, P.; Dannenberg, J. J.; Zakrzewski, V. G.; Dapprich, S.; Daniels, A. D.; Strain, M. C.; Farkas, O.; Malick, D. K.; Rabuck, A. D.; Raghavachari, K.; Foresman, J. B.; Ortiz, J. V.; Cui, Q.; Baboul, A. G.; Clifford, S.; Cioslowski, J.; Stefanov, B. B.; Liu, G.; Liashenko, A.; Piskorz, P.; Komaromi, I.; Martin, R. L.; Fox, D. J.; Keith, T.; Al-Laham, M. A.; Peng, C. Y.; Nanayakkara, A.; Challacombe, M.; Gill, P. M. W.; Johnson, B.; Chen, W.; Wong, M. W.; Gonzalez, C.; Pople, J. A. *Gaussian 03*, revision C.02; Gaussian, Inc.: Wallingford, CT, 2004.
(20) Peng, C.; Ayala, P. Y.; Schlegel, H. B. *J. Comput. Chem.* **1996**, *17* (1), 49−56.
(21) Peng, C.; Schlegel, H. B. *Israel. J. Chem.* **1993**, *33*, 449−454.
(22) Gonzalez, C.; Schlegel, H. B. *J. Chem. Phys.* **1989**, *90* (4), 2154−2161.
(23) Becke, A. *J. Chem. Phys.* **1993**, *98* (7), 5648−5652.
(24) Coote, M. L.; Wood, G. P. F.; Radom, L. *J. Phys. Chem. A* **2002**, *106* (50), 12124−12138.
(25) Montgomery, J. A.; Frisch, M. J.; Ochterski, J. W.; Petersson, G. A. *J. Chem. Phys.* **1999**, *110* (6), 2822−2827.
(26) Baboul, A. G.; Curtiss, L. A.; Redfern, P. C. *J. Chem. Phys.* **1999**, *110* (16), 7650−7657.
(27) Curtiss, L. A.; Redfern, P. C.; Raghavachari, K.; Rassolov, V.; Pople, J. A. *J. Chem. Phys.* **1999**, *110* (10), 4703−4709.
(28) Scott, A.; Radom, L. *J. Phys. Chem.* **1996**, *100* (41), 16502−16513.
(29) Van Speybroeck, V.; Van Neck, D.; Waroquier, M.; Wauters, S.; Saeys, M.; Marin, G. B. *J. Phys. Chem. A* **2000**, *104*(46), 10939−10950.
(30) Cancés, E.; Mennucci, B.; Tomasi, J. *J. Chem. Phys.* **1997**, *107* (8), 3032−3041.
(31) Rappé, A.; Casewit, C.; Colwell, K.; Goddard, W.; Skiff, W. *J. Am. Chem. Soc.* **1992**, *114* (25), 10024−10035.
(32) McQuarrie, D. A.; Simon, J. D. *Molecular Thermodynamics*; University Science Books: Sausalito, CA, 1999.
(33) Frenkel, M.; Marsh, K. N.; Wilhoi, R. C.; Kabo, G. J.; Roganov, G. N. *Thermodynamics of Organic Compounds in the Gas State*; Thermodynamics Research Center: College Station, TX, 1994; Vol. 1.
(34) Sumathi, R.; Carstensen, H.; Green, W. H., Jr. *J. Phys. Chem. A* **2001**, *105* (28), 6910−6925.
(35) Marston, C. C.; Balint-Kurti, G. G. *J. Chem. Phys.* **1989**, *91* (6), 3571−3576.
(36) Balint-Kurti, G. G.; Dixon, R.; Marston, C. C. *Int. Rev. Phys. Chem.* **1992**, *11*, 317−344.
(37) Balint-Kurti, G. G.; Ward, C. L.; Marston, C. C. *Comput. Phys. Commun.* **1991**, *67*, 285−292.
(38) Sebbarand, N.; Bockhorn, H.; Bozzelli, J. W. *J. Phys. Chem. A* **2005**, *109* (10), 2233−2253.
(39) Cauter, K. V.; Speybroeck, V. V.; Vansteenkiste, P.; Reyniers, M. F.; Waroquier, M. *ChemPhysChem* **2006**, *7*, 131−140.
(40) Hirschfelder, J. O.; Wigner, E. J. *J. Chem. Phys.* **1939**, *7* (8), 616−628.
(41) Gonzalez-Lafont, A.; Truong, T. N.; Truhlar, D. G. *J. Chem. Phys.* **1991**, *95* (12), 8875−8894.
(42) Zhang, S.; Truong, T. N. VKLab version 1.0. University of Utah, 2001.
(43) Brinck, T.; Lee, H.; Jonsson, M. *J. Phys. Chem. A* **1999**, *103* (35), 7094−7104.
(44) Redfern, P. C.; Zapol, P.; Curtiss, L. A.; Raghavachari, K. *J. Phys. Chem. A* **2000**, *104* (24), 5850−5854.
(45) Truong, T. N.; Duncan, W.; Tirtowidjojor, M. *Phys. Chem. Chem. Phys.* **1999**, *1* (6), 1061−1065.
(46) Henry, D. J.; Radom, L. In *Quantum-Mechanical Prediction of Thermochemical Data*; Understanding Chemical Reactivity; Cioslowski, J., Ed.; Kluwer Academic Publishers: Norwell, MA, 2001; Vol. 22, pp 161−197.
(47) Avila, D. V.; Ingold, K. U.; Lusztyk, J.; Green, W. H., Jr.; Procopio, D. R. *J. Am. Chem. Soc.* **1995**, *117* (10), 2929−2930.
(48) Broadbelt, L. J.; Pfaendtner, J. *AIChE J.* **2005**, *51* (8), 2112−2121.
(49) Van Geem, K. M.; Reyniers, M. F.; Marin, G. B.; Song, J.; Green, W. H., Jr.; Matheu, D. M. *AIChE J.* **2006**, *52* (2), 718−730.